REGULAR PAPER

Investigation on MRR and Machining Gap of Micro Reciprocated Wire-EDM for SKD11

Xiang Chen[1] · Zhenlong Wang[1,2] · Yukui Wang[1,2] · Guanxin Chi[1]

Abstract

In this paper, the investigational work is carried out on the micro reciprocated wire electrical discharge machining (wire-EDM) of SKD11 using circularly travelled wire with Φ30 μm as tool electrode, aiming to achieve the fabrication of micro parts with high cost-effect, efficiency and precision. The experiments are systematically performed using central composite design approach of response surface methodology to study the effect of open voltage, discharge capacitance, pulse duration and feed rate on material removal rate (MRR) and machining gap. The mathematical models of MRR and machining gap are developed by analysis of variance, and whilst verified by confirmation experiments with ≤ 8.38% and 6.70% prediction errors for MRR and machining gap, respectively. Besides, multi-objective optimization of parameter combinations is attempted by non-dominated sorting genetic algorithm-II. Finally, a typical experimental sample, micro gear is successfully machined with 1194.38 μm tip diameter under the condition of No. 14 optimal solution.

Keywords Micro reciprocated wire-EDM · SKD11 · CCD · MRR · Machining gap · NSGA-II

List of symbols

U Open voltage
C Discharge capacitance
T_{on} Pulse duration
F Feed rate
T_{off} Pulse interval
R Discharge resistance

1 Introduction

With the rapid development of micro-electromechanical systems (MEMS) and micro systems technology (MST), the demand for large amounts of micro components or devices is dramatically increasing [1]. Thereinto, the micro molding technology provides a feasible method to achieve the mass production of micro parts [2, 3]. Whereas, the material properties of the micro molds must be deliberately considered

to meet different application requirements. Considering the high energy-efficiency and forming precision especially for micro scale part, the precision cold forming is very suitable for machining micro components [4]. In this case, SKD11 die steel in Japanese specification is one of the most appropriate materials due to its characteristics of high strength and toughness, good wear-resistance and excellent heat balance [5].

However, this kind of material is difficult to be machined by conventional manufacturing processes such as turning, drilling and milling. Thus, non-conventional machining technologies can be employed, including lithography, electroplating, and molding (LIGA), micro electrical discharge machining (micro-EDM), micro electrochemical machining (micro-ECM) and laser processing etc. Compared with the above technologies, micro reciprocated wire electrical discharge machining (wire-EDM) provides a promising alternative to fabricate the micro molds made from SKD11 due to its distinctive superiorities of high machining accuracy, cost-effective and non-contact machining on difficult-to-cut metal materials [6–8]. When machining micro molds by micro reciprocated wire-EDM, much attention should be paid to processing accuracy because it plays a critical role in determining forming precision [9]. On the other hand, the machining efficiency is also significant for the rapid production of various molds. However, the two performances are

✉ Yukui Wang
   wangyukui@hit.edu.cn

1   School of Mechatronics Engineering, Harbin Institute of Technology, Harbin 150001, China

2   Key Laboratory of Micro-systems and Micro-structures Manufacturing of Ministry of Education, Harbin Institute of Technology, Harbin 150001, China

in conflict with each other in micro reciprocated wire-EDM process [10]. The investigation and optimization on machining performance and processing parameters for SKD11 attract many researchers' attention.

Zhao et al. [11] studied the WEDM process of SiC and SKD11, and found that under the same machining condition, the *MRR* and tool wear ratio of SiC were superior to that of SKD11. Ming et al. [12] investigated the energy distribution ratio during the EDM of Al 6061, Inconel 718 and SKD11, and found that the discharge energy transferred to the three kind of workpiece were all small. Zheng [13] analyzed the energy characteristics in WEDM, and established a non-pulsed auxiliary energy costing and feeding energy prediction model to save energy. An attempt had been conducted to obtain good surface quality in LS-WEDM process, and it was found that the high rotating speed and peak current generated poor surface quality [14]. Other investigations have also been conducted for high machining accuracy. Based on the analysis between the kerf width and machining parameters, Di et al. [15] established the mathematical model of wire lateral vibration and cut 30.8 μm width slot on stainless steel. The wire movement in fine wire-EDM process was recorded using high-speed camera and the wire vibration was also analyzed under different machining condition, it was found that the machining accuracy could be improved by increasing offset [16], and arranging the workpiece at the position of 3rd order node [17].

In order to find the optimal solutions of the machining performance and parameters, many researches have been carried out. The hybrid approach combining grey relational analysis with principle component analysis was used to identify the optimal parameters for the WEDM process of nanostructured hardfacing material [18]. The production efficiency and part quality of alloy steel was improved by multi-objective optimization of machining parameters based on artificial neural networks [19]. The high material removal rate with better surface finish was obtained by multi-objective genetic algorithm for machining nickel-titanium-based shape memory alloy [20]. According to the above summary, it is found that the systematic investigation on MRR and machining gap for machining SKD11 by micro reciprocated wire-EDM has not been given yet.

In this paper, the effects of open voltage, discharge capacitance, pulse duration and feed rate on MRR and machining gap of SKD11 are studied by the experiments designed based on central composite design (CCD) of response surface method (RSM). The mathematical models for the two responses have been developed, and whilst verified through confirmation experiments. Furthermore, the multi-objective optimization of the machining parameters is conducted using the improved non-dominated sorting genetic algorithm (NSGA-II) for different machining performances. Based on the above systematical investigation, a typical experimental

sample, micro gear is successfully machined with high machining efficiency and accuracy using one of the optimal machining conditions.

2 Experimental Detail

2.1 Experimental Setup

Figure 1 shows the photograph of micro-WEDM setup with reciprocated traveling wire electrode. It mainly consists of reciprocated wire-moving system, RC micro energy pulse generator with precise control, servo control system based on piezoelectric ceramics motors drive, constant tension control unit, vibration inhibition unit, working liquid-circulation system and CCD camera system. The X/Y stage with 0.1 μm in resolution is composed of precise servomotor and driver which is driven by piezoelectric ceramic motors, utilizing a high-precision grating ruler as the position feedback component. Because the micro energy generator is utilized and the ultrafine wire electrode is circularly travelling, the wear of wire electrode is negligible. The working liquid-circulation system is used to cool electrodes and expel the debris particles from the machining gap easily, and the CCD camera system is applied to observe the micro-WEDM process.

2.2 Experimental Material

The material employed in this study is SKD11 in Japanese specifications considering its properties of high hardness and toughness, good hardenability, as well as excellent wear-resistance and thermostability. Its harness is 56–58 HRC, impact toughness is 9.1 J cm^{-2} and other mechanical properties are given in Table 1. The as-received workpiece is a plate with 2 mm thickness. To avoid the overcut of the fillet
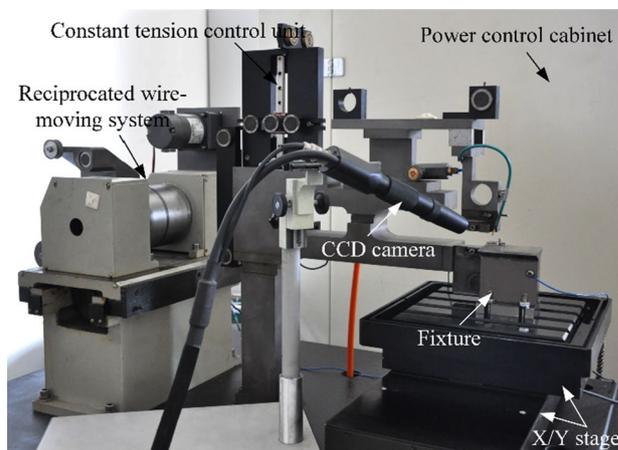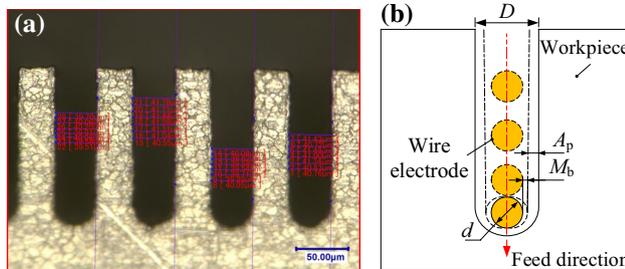

Fig. 1 Micro reciprocated wire-EDM setup

Table 1 Mechanical properties of SKD11

Mechanical properties	Values
Hardness (HRC)	56–58
Impact toughness (J cm^{-2})	9.1
Tensile strength (MPa)	≥ 600
Yield strength (MPa)	≥ 355

Fig. 2 Measurement and analysis for the kerf width: **a** partly machined kerf and **b** schematic diagram of the machined kerf

radius, the tool electrode used in experiments is the ultrafine tungstenic wire with 30 μm diameter, which has high melting point of 3410 °C and stable chemical properties. Commercial EDM oil is used as working medium because of the good deionization insulation.

2.3 Evaluation for MRR and Machining Gap

The experiments are performed on SKD11 plate with 2 mm thickness. The cutting length is 120 μm in each experiment. The micro wire with 30 μm diameter is selected as tool electrode in all tests. *MRR* is expressed by the removed volume of SKD11 material in unit time, as shown in Eq. (1).

$$MRR = \text{Removed volume} \big/ \text{Machining time} \tag{1}$$

The microscope system VHX-6000 made by KEYENCE is applied to measure the kerf width, and seven measurements are conducted for each slot along the cutting direction as shown as the red part in Fig. 2a. The average value of every kerf width is calculated as the final value. Figure 2b indicates the schematic diagram of the cut kerf. When the distance M_b becomes small enough, the dielectric fluid in the clearance will be broke down by the voltage between the wire electrode and workpiece, and simultaneously the discharge happens. The discharge force is randomly exerted on the micro wire, causing the micro wire to vibrate in the discharge gap. The maximum amplitude of the wire lateral vibration is represented by A_p. When the micro wire (diameter d) is selected, the kerf width D is mainly determined by the breakdown gap M_b and the wire lateral vibration A_p, which can be expressed as Eq. (2).

$$D = d + 2(M_b + A_p) \tag{2}$$

The breakdown gap M_b is mainly determined on the electric field intensity and insulation medium between the two electrodes. But, it is difficult to be calculated because the breakdown condition is affected by the purity of the insulation medium. Besides, the magnitude, occurrence time and location of the discharge force acting on the micro wire is very complicated, thus the wire lateral vibration A_p cannot be easily figured out. According to Eq. (2), the algebraic sum of M_b and A_p can be easily calculated when the kerf width D and wire diameter d are obtained. That is defined as the machining gap M_g and expressed in Eq. (3).

$$M_g = (D - d) \big/ 2 \tag{3}$$

3 Experimental Design and Optimization

3.1 Experimental Design

During micro reciprocated wire-EDM, *MRR* is the main machining characteristic reflecting the processing efficiency. The machining accuracy of the machined micro tools has significant influence on the subsequent application, and it can be represented by machining gap. Thus, *MRR* and machining gap are mainly discussed in this paper. However, a challenge is caused because *MRR* and machining gap must be considered simultaneously. The mathematical model should be established in order to predict the two responses under any given input factors. To improve the predicting capability of the established models, the reasonable input factors have to be properly selected. Because the RC micro-energy pulse power is used in the study, the open voltage and discharge capacitance affect the single pulse discharge energy. Besides, the pulse duration determines the discharge time and the feed rate influences the discharge frequency. Therefore, the above four parameters are chosen as the input factors. Based on the literature survey [21], machine capability and many preliminary studies, the levels of the four input factors and other constant parameters are shown in Table 2.

Response surface methodology (RSM) was originally developed by Box and Wilson to explore the potentials of statistical design in industrial experiments [22]. The experimentation along with the regression analysis facilitates the development of the mathematical model between the desired response and the input factors. In RSM, the mathematical relationship of the output responses versus the input factors can be expressed by Eq. (4):

$$y_i = f(x_1, x_2, x_3, \ldots, x_n) \pm \varepsilon \tag{4}$$

where y_i is the desired response, f is the response function and $x_1, x_2, x_3, \ldots, x_n$ are the input parameters, ε is the fitting error which measures the experimental errors. In generally,

Table 2 Processing conditions in micro wire-EDM process[21]

Parameters	Value
Open voltage U (V)	60 (low level)–140 (high level)
Discharge capacitance C (pF)	1470 (low level)–3000 (high level)
Pulse duration T_{on} (μs)	0.5 (low level)–16 (high level)
Feed rate F (μm min^{-1})	17.8 (low level)–48 (high level)
Pulse interval T_{off} (μs)	20
Discharge resistance R (kΩ)	500
Working medium	Kerosene
Polarity	Positive (workpiece)

the quadratic model is proposed to present the approximation of the response function, which can be expressed as following:

$$y_i = a_0 + \sum_{i=1}^{n} a_i x_i + \sum_{i=1}^{n} a_{ii} x_i^2 + \sum \sum_{i<j}^{n} a_{ij} x_i x_j \pm \varepsilon \tag{5}$$

where a_0 is the constant term determined by the method of least squares, a_i, a_{ii} and a_{ij} represent the coefficients of liner, quadratic and interactive terms, respectively. The response y_i may include linear, quadratic and interaction terms.

The central composited design (CCD) fits the quadratic responses very accurately. Besides, it is widely used in various RSM designs due to its advantages of high flexibility and efficiency in providing the overall experimental error in minimum tests. Therefore, it is employed to design the experiments in this study. The experimental design matrix and the responses are shown in Table 3.

3.2 Optimization Technique

NSGA-II is one of the most popular multi-objective genetic algorithms because it has the advantages of high running speed and good convergence of the solution set. Thus, it is used to obtain the objectives of maximum *MRR* and

Table 3 Experimental design matrix and relevant responses

Test no.	U (V)	C (pF)	T_{on} (μs)	F (μm/min)	MRR (10^5 μs^3/min)	M_g (μm)
1	100	2985	8.25	32.90	6.974	4.96
2	140	4500	0.50	48.00	8.579	5.28
3	60	4500	16.00	17.80	2.319	4.68
4	140	1470	0.50	48.00	7.816	4.58
5	100	6015	8.25	32.90	7.814	5.22
6	100	2985	8.25	32.90	6.942	5.01
7	20	2985	8.25	32.90	2.496	4.02
8	60	1470	0.50	17.80	1.15	3.69
9	100	2985	8.25	32.90	6.895	5.01
10	100	2985	8.25	32.90	6.853	4.76
11	100	2985	8.25	32.90	6.889	4.86
12	140	4500	0.50	17.80	6.592	5.70
13	140	1470	0.50	17.80	5.593	5.14
14	100	2985	0.15	32.90	5.578	4.20
15	100	450	8.25	32.90	5.848	4.48
16	60	1470	16.00	17.80	1.67	4.38
17	140	1470	16.00	48.00	8.378	5.23
18	140	1470	16.00	17.80	6.962	5.66
19	60	1470	16.00	48.00	3.214	3.76
20	100	2985	23.75	32.90	7.535	5.29
21	100	2985	8.25	63.10	8.584	4.37
22	100	2985	8.25	2.70	5.178	5.21
23	180	2985	8.25	32.90	8.52	5.17
24	60	4500	0.50	17.80	1.922	4.42
25	60	4500	16.00	48.00	3.74	4.27
26	140	4500	16.00	17.80	7.944	6.08
27	100	2985	8.25	32.90	6.874	4.93
28	140	4500	16.00	48.00	8.997	5.63
29	60	1470	0.50	48.00	2.427	3.33
30	60	4500	0.50	48.00	3.519	4.02

minimum machining gap in this paper. The two responses are the functions of input factors and will be discussed in Sects. 4.1 and 4.2. NSGA-II is an improved multi-objective genetic algorithm based on NSGA, proposed by Dev et al. [23]. The procedure of multi-objective optimization using NSGA-II is shown in Fig. 3. Specifically, the initially parent population P of size N is randomly generated. Then, offspring Q of size N generated through the genetic operation including selection, crossover and mutation, which is created from parents by simulated binary crossover. The random mutation operator is used to create a solution from the entire search space. When the objective function of all individuals in R has been combined parent P and offspring Q, the solutions for the objective function are sorted into diverse nondominated fronts. The better solutions are chosen based on the crowded comparison operator for better new population P. The above process is repeated until the required generation is reached. In this paper, the initial population size N with 100 and the maximum generation with 200 is used for better convergence and efficiency.

response and the input factors is established using RSM. In this paper, the statistical analysis software of Designer-Expert 8.0 is applied to compute the regression coefficients of the developed models. The analysis of variance (ANOVA) technique is employed to find out the factors and the interaction between various factors that have significant impact on the responses. The "P value" in ANOVA result is used to check the appropriateness and significance of the model by judging if it is less than 0.05 and 0.001, respectively. From the ANOVA result of MRR in Table 4, it can be seen that the "P value" for the model is < 0.0001, which indicates that the model is significant. Besides, the "P value" of the terms including A, B, C, D, A^2, C^2 are less than 0.05, revealing that they are statistically significant for MRR model. Other terms with the "P value" of larger than 0.05 are not significant and can be removed from the MRR model. The final simplified equation for MRR model is expressed in Eq. (6).

$$MRR = 12.3802 + 0.2456 \times U + 0.0003 \times C + 0.16278 \times T_{on} + 0.058587 \times F - 0.000902 \times U^2 - 0.006571 \times T_{on}^2 \tag{6}$$

4 Results and Discussions

4.1 Analysis of MRR for Machining SKD11

To analyze the machining process and optimize the machining parameters, a mathematical model between the output
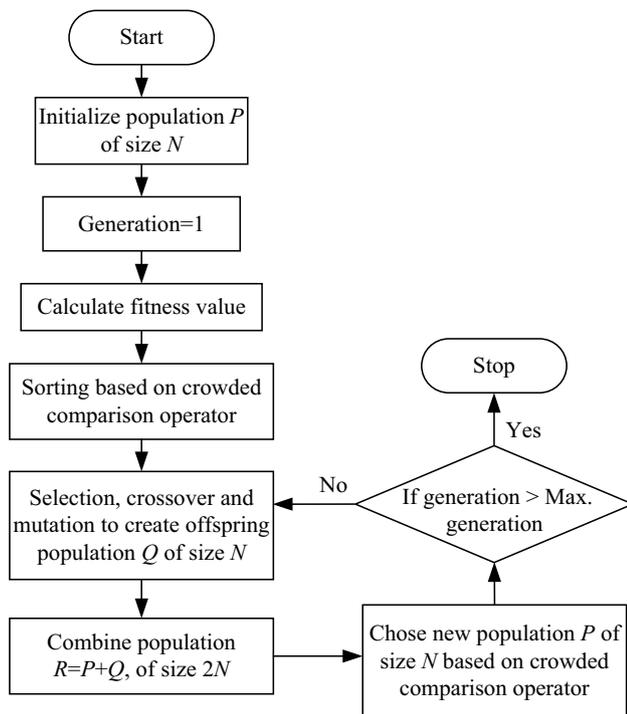

Fig. 3 Flow chart of multi-objective optimization using NSGA-II

Table 4 ANOVA results of MRR

Source	Sum of squares	DF	Mean square	F-value	P value
Model	166.03	14	11.86	51.09	< 0.0001
A—U	122.33	1	122.33	526.94	< 0.0001
B—C	3.89	1	3.89	16.76	0.0010
C—T_{on}	3.19	1	3.19	13.76	0.0021
D—T_{off}	14.09	1	14.09	60.68	< 0.0001
AB	6.56E−3	1	6.56E−3	0.028	0.8687
AC	0.20	1	0.20	0.85	0.3714
AD	0.044	1	0.044	0.19	0.6691
BC	0.045	1	0.045	0.19	0.6655
BD	0.010	1	0.010	0.044	0.8376
CD	0.17	1	0.17	0.73	0.4054
A^2	5.08	1	5.08	21.87	0.0003
B^2	0.015	1	0.015	0.066	0.8011
C^2	0.32	1	0.32	1.38	0.0258
D^2	1.86E−3	1	1.86E−3	7.99E−3	0.9299
Residual	3.48	15	0.23		
Lack of fit	3.47	10	0.35	171.04	0.3175
Pure error	0.010	5	2.03E−3		
Core total	169.52	29			
SD	0.48		R-Squared	0.9795	
Mean	5.79		Adj R-Squared	0.9603	
C.V. %	8.32		Pred R-Squared	0.9043	
PRESS	16.23		Adeq Precision	25.699	

The lack of fit is a measure to evaluate whether the model is adequate or not. The model is inadequate if there is a significant lack of fit [24]. The "*P* value" of lack of fit is 0.3175, implying that the lack of fit is insignificant and the *MRR* model is advisable. The "Predicted R-square" of 0.9043 is in reasonable agreement with the "Adjust R-square" of 0.9603. All the data show that the *MRR* model provides good accuracy. The normal probability plot of the residuals for *MRR* is shown in Fig. 4. It can be observed that the residuals generally fall on a straight line, which implies that the errors are normally distributed.

The perturbation plot in Fig. 5 shows the comparative effects of open voltage (A), discharge capacitance (B), pulse duration (C) and feed rate (D) on *MRR*. By default, Design Expert 8.0 software sets the reference point at the midpoint (coded value 0) of all factors. It can be seen from Fig. 5 that *MRR* increases rapidly with open voltage increase in the initial stage, but it tends to be stable when open voltage reaches a certain level. The reason is that *MRR* depends on the discharge energy which is mainly determined by open voltage. The high value of open voltage will lead to much material to be removed. However, when the open voltage increases to a certain value, the single discharge energy is so large that much material are removed and the generated debris particles are accumulated in the discharge gap, thus deteriorating the discharge state and decreasing *MRR*. The rise in discharge capacitance causes the increase of *MRR*. The reason for the phenomenon is in the same way as that of open voltage, but *MRR* is less sensitive to discharge capacitance than open voltage. As for the plot of pulse duration and *MRR*, the large value of pulse duration results in high *MRR*. It can be explained that the pulse duration increases the discharge time, which causes a large amount of discharge energy. The high feed rate generates large *MRR*. The reason
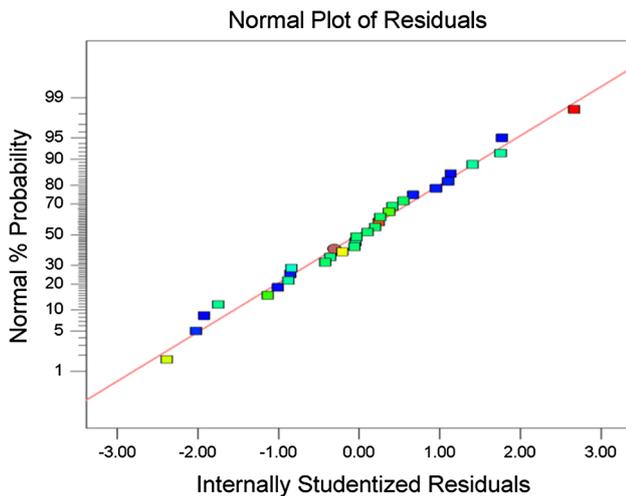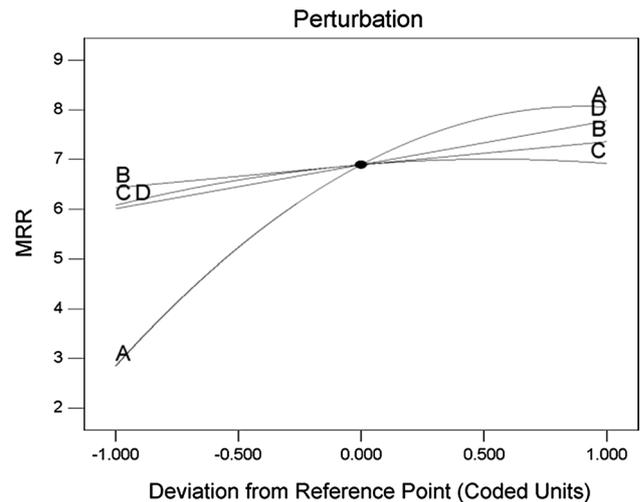

Fig. 5 Perturbation plot of *MRR*

is that the high feed rate increases the discharge frequency, thus increasing the *MRR*.

4.2 Analysis of Machining Gap for Machining SKD11

ANOVA is performed using Designer-Expert 8.0 software to statistically analyze the results of machining gap model, individual model terms and lack of fit. The ANOVA result of the machining gap for machining SKD11 is shown in Table 5. It can be observed that the "*F*-value" of machining gap model is 96.94, which indicates that there is only a 0.01% chance that a "Model *F*-value" this large could occur due to noise. The model term is significant if it's "*P* value" is less than 0.05. In this case, the terms A, B, C, D, BC and A^2 are significant for machining gap model. The "*P* value" of "Lack of fit" is 0.1670, implying that the lack of fit is insignificant. Non-significant lack of fit is good because it enables the model to match the experimental data. The determination coefficient "R-squared" is 0.9620, which indicates that the quadratic model can explain 96.20% variation in the machining gap. The "Pred R-Squared" of 0.9444 is in reasonable agreement with the "Adj R-Squared" of 0.9520. The "Adeq Precision" measures the signal to noise. The value of 42.111 for "Adeq Precision" indicates an adequate signal because a ratio larger than 4 is desirable. Therefore, the quadratic model of machining gap can be used to navigate the design space. The developed quadratic model for the machining gap is expressed in Eq. (7).

$$M_g = 1.9456 + 0.0332 \times U + 0.00023 \times C + 0.04973 \times T_{on}$$
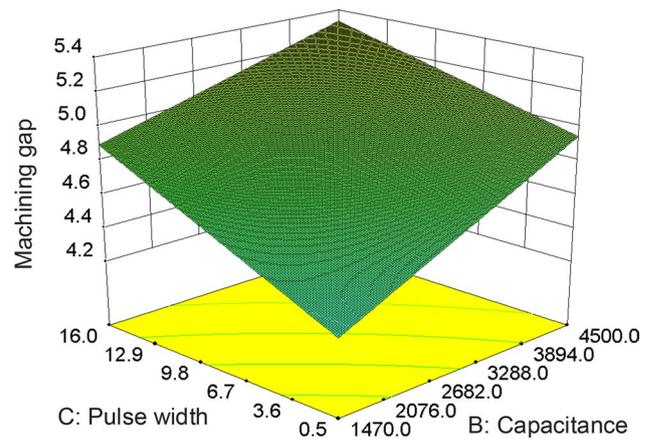$$- 0.0166 \times F - 0.0000558 \times C \times T_{on} - 0.0000838 \times U^2$$
$$(7)$$

From Eq. (7), it is found that there is interaction between capacitance and pulse width on machining gap. The

Fig. 4 Normal plot of residuals for *MRR*

Table 5 ANOVA of machining gap for machining SKD11

Source	Sum of squares	DF	Mean square	F value	P value
Model	11.83	14	0.84	96.94	<0.0001
A- U	7.87	1	7.87	272.43	<0.0001
B- C	1.42	1	1.42	49.23	<0.0001
C- T_{on}	1.18	1	1.18	40.92	<0.0001
D- T_{off}	1.12	1	1.12	38.93	<0.0001
AB	1.56E−3	1	1.56E−3	0.054	0.8194
AC	5.18E−3	1	5.18E−3	0.18	0.6779
AD	2.33E−4	1	2.33E−4	8.05E−3	0.9297
BC	0.069	1	0.069	2.38	0.0143
BD	5.70E−3	1	5.70E−3	0.20	0.6632
CD	1.85E−3	1	1.85E−3	0.064	0.8037
A^2	0.081	1	0.081	2.82	0.0113
B^2	0.015	1	0.015	0.51	0.4857
C^2	2.26E−3	1	2.26E−3	0.078	0.7837
D^2	4.89E−4	1	4.89E−4	0.017	0.8982
Residual	0.43	15	0.029		
Lack of fit	0.39	10	0.039	2.46	0.1670
Pure error	0.047	5	9.46E−3		
Core total	12.26	29			
SD	0.14		R-Squared	0.9620	
Mean	4.78		Adj R-Squared	0.9520	
C.V. %	2.98		Pred R-Squared	0.9444	
PRESS	0.68		Adeq Precision	42.111	

Fig. 6 Interaction of pulse width and capacitance on machining gap under 100 V open voltage and 32.9 μm/min feed rate

variation of machining gap under the interaction of the two factors can be obtained by Design Expert software, and the result is shown in Fig. 6. It presents that when other conditions remain unchanged, the machining gap increases with the increase of pulse width and capacitance. The reason is that the discharge energy is proportional to capacitance, and the pulse width determines the discharge time. Thus, the discharge energy will be increased when using large capacitance and pulse width, leading to the severe vibration of micro wire.

Figure 7 presents the normal probability plot of the residuals for machining gap, and it is observed that the residuals are lying on a straight line, which means that the errors are normally distributed. Figure 7 shows the perturbation plot of machining gap versus open voltage (A), discharge capacitance (B), pulse duration (C) and feed rate (D). The large slope for open voltage and feed rate indicate that the machining gap is highly sensitive to the two factors while the relative flat lines for discharge capacitance and pulse duration means that the machining gap is less sensitive to these factors. It can be observed from Fig. 8 that the machining gap increases with the rise in open voltage. On one hand,

the single discharge energy increases when using high open voltage, and that causes large discharge force and electromagnetic force, thus resulting in fierce wire vibration. On the other hand, the breakdown gap between micro wire and workpiece is proportional to open voltage [25, 26], thus generating larger machining gap. The above two factors result in this phenomenon. The effects of discharge capacitance and pulse duration on machining gap are in the same way as open voltage. The reason for the phenomenon is the same as the first one of open voltage. But the machining gap is less sensitive to discharge capacitance and pulse duration compared with open voltage. As for the effect of feed rate on machining gap, the increase in feed rate leads to the decrease of machining gap. The reason is that when using low feed rate, the discharge frequency is so low that the single pulse discharge force is large and exerts much influence on the
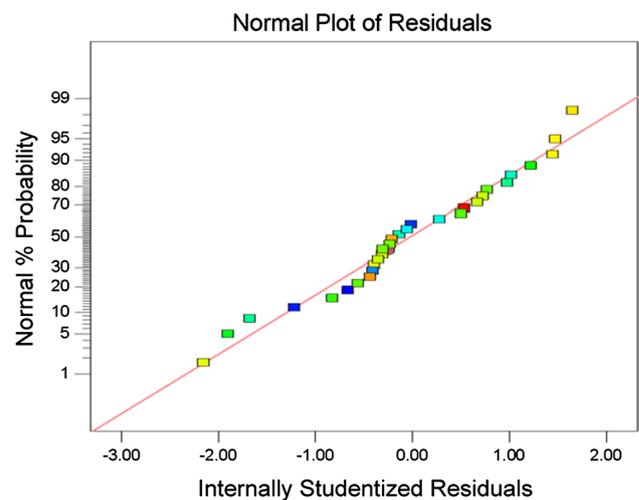
Fig. 7 Normal plot of residuals for machining gap

Fig. 8 Perturbation plot of machining gap
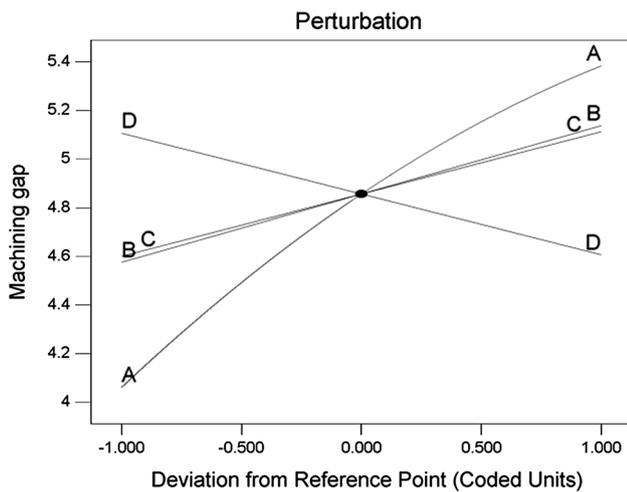
Fig. 9 **a** Experimental and predicted results for *MRR* and **b** Experimental and predicted results for machining gap
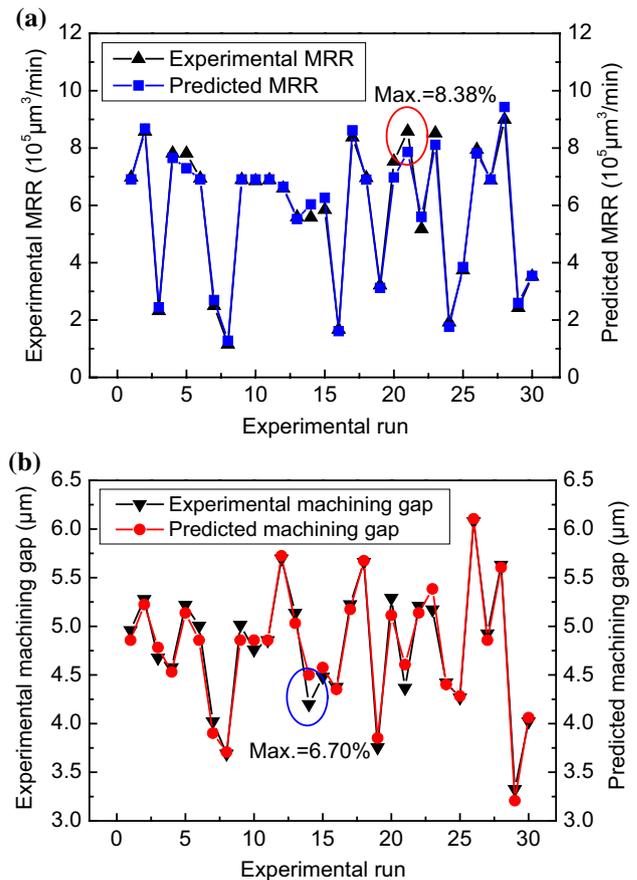
micro wire vibration. With the increase of feed rate, the discharge frequency increases and the single pulse discharge force decreases, thus reducing the vibration amplitude of the micro wire.

4.3 Comparison of Experimental and Predicted Responses

Confirmation experiments are performed for 30 experiments to validate the quadratic models of *MRR* and machining gap expressed in Eqs. (6) and (7), respectively. The experimental conditions are the same as that in Table 3. Every experiment is performed three times and the average value is calculated as the final result of each run. The comparison between the experimental and predicted results for *MRR* and machining gap is shown in Fig. 9a, b. It is noted that the experimental *MRR* and machining gap are following the predicted values calculated from the developed models. The relative deviation between the experimental and predicted results for *MRR* and machining gap are respectively figured out. It is found that the maximum deviation rate of *MRR* is 8.38%, and that of machining gap is 6.70%. According to the above results, it can be concluded that the developed models of *MRR* and machining gap are reliable, and they can be used for the advance prediction for the purpose of high efficiency and accuracy.

4.4 Multi-objective Optimization Based on NSGA-II

In order to obtain the best fitness values of the objective function, NSGA-II is implemented by the codes written in MATLAB R2015b. The codes have been implemented using eight different functions to conduct the steps in NSGA-II. For better convergence, the population size *N* with 100 and the generation number with 200 are entered

as the input augments to the functions. A set of 100 non-dominated solutions are obtained finally. Figure 10 shows the pareto-optimal front i.e. the final set of solutions. Because the performance studied in this paper are conflicting in nature, the machining accuracy decreases with the increase of *MRR*. The same performance characteristic can be clearly observed in the obtained solutions presented in Fig. 10. The partial objective fitness values and their decision variables of non-dominated solution are enlisted in Table 6. Since none of the solutions in the pareto-optimal set is completely superior to others, any one of them can be acceptable. The selection of one solution depends on the working requirement. The solutions in Region-A will be selected if the machining accuracy is more desirable than *MRR*. Accordingly, *MRR* is compromised due to the conflicting nature of the two responses. The solutions in Region-C are suitable if *MRR* is more desirable than machining gap. But the machining accuracy will be compromised at the same time. The solutions in Region-B should be considered if the machining accuracy and *MRR* are treated equally.
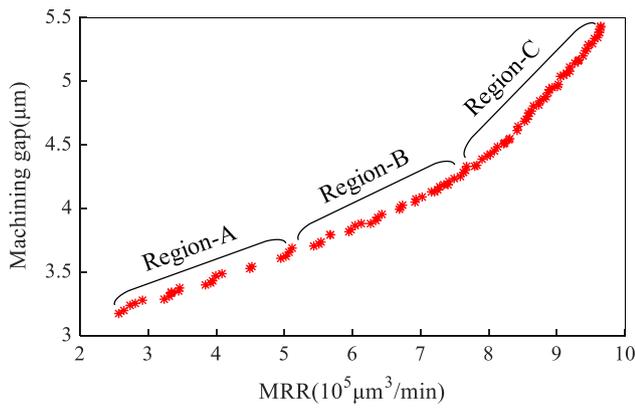
Fig. 10 Pareto-optimal front between *MRR* and machining gap

4.5 Application of Optimal Solutions

A micro gear with the tip diameter of 1200 μm and the module of 10 is chosen as the machining sample. To keep the balance between high *MRR* and good machining accuracy, the solution labelled No. 14 is selected to fabricate the experimental sample. The actual machining gap is 3.83 μm obtained under No. 14 processing condition, and whilst it is compensated in the tool path planned by UG NX 8.0 software. The tool paths without and with compensating machining gap are presented in Fig. 11a, b, and the relevant machined samples are shown in Fig. 12a, b, respectively. The tip diameters of the two samples are measured by VHX-6000 on five pair of teeth, and the average values are 1186.64 μm and 1194.38 μm, respectively. It can be noted that the deviation of the two samples is 7.74 μm, which is nearly the same as the double machining gap under No. 14 solution.

**Table 6** Pareto-optimal solutions (only 30 solutions are given)

No.	U (V)	C (pF)	T_{on} (μs)	F (μm/min)	MRR (10^5 μm³/min)	M_g (μm)
1	60	1480	0.5	50	2.570	3.18
2	135	4460	12.5	50	9.639	5.42
3	75	1570	1	50	4.531	3.55
4	70	1980	0.5	50	4.007	3.52
5	80	1570	0.5	50	4.984	3.63
6	70	1460	0.5	50	3.847	3.39
7	65	1570	1.5	49.4	3.376	3.36
8	80	1570	1	50	5.060	3.65
9	80	1570	2.5	50	5.269	3.71
10	120	2600	6.5	50	8.607	4.74
11	90	1570	2.5	50	6.192	3.90
12	105	1570	1	50	7.028	4.09
13	120	2590	8	50	8.705	4.79
14	85	1570	2	50	5.687	3.79
15	120	1570	5.5	50	8.207	4.49
16	60	1570	3	50	2.947	3.30
17	100	1570	1.5	50	6.797	4.03
18	90	1470	1.5	49	5.966	3.86
19	110	1570	0.5	50	7.209	4.15
20	110	1570	1	50	7.286	4.17
21	80	1570	3	50	5.333	3.73
22	115	1570	6	50	8.083	4.45
23	120	3250	10	50	8.997	4.98
24	130	1570	7	50	8.529	4.68
25	135	4460	10.5	50	9.616	5.37
26	120	3340	8	50	8.934	4.93
27	65	1570	0.5	50	3.262	3.31
28	85	1570	1	50	5.544	3.75
29	90	1570	0.5	50	5.906	3.82
30	95	1570	1	49.6	6.352	3.94
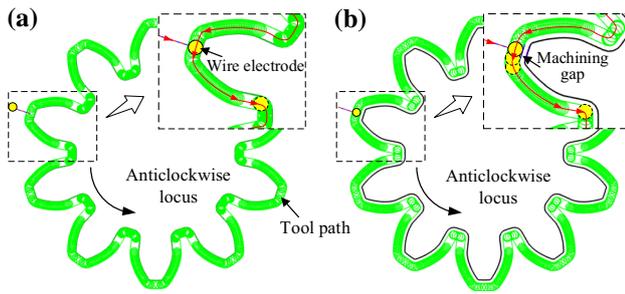
Fig. 11 Tool path of the micro gear: **a** without compensating machining gap and **b** with compensating machining gap
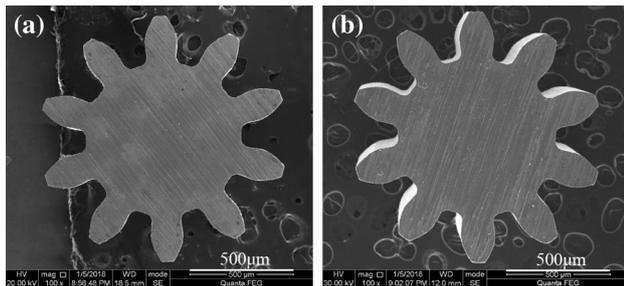

Fig. 12 Machined micro gear: **a** without compensating machining gap and **b** with compensating machining gap
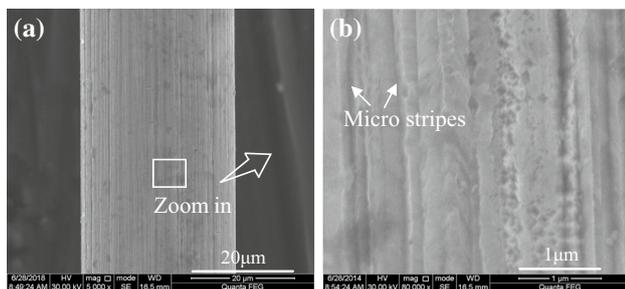
Fig. 13 SEM images of micro wire before machining: **a** overall view and **b** enlarged view

To understand the wear of the repeatedly used micro wire, the new micro wire before machining and the used one continuously working about 17 h to fabricate micro gear are inspected by scanning electron microscopy and microscope system VHX-6000, respectively. Figure 13a shows the smooth surface of new micro wire. There are some micro stripes on the surface along the axial direction of new micro wire as shown in Fig. 13b, which are formed in the drawing process of wire electrode. From Fig. 14a, it can be seen that there is no large wear on the used micro wire due to using micro-energy power supply in micro-WEDM. However, there are many eroded pits on the surface of the micro wire after machining micro gear as shown in Fig. 14b. Nevertheless, the diameters of the micro pits are within 2 μm, and
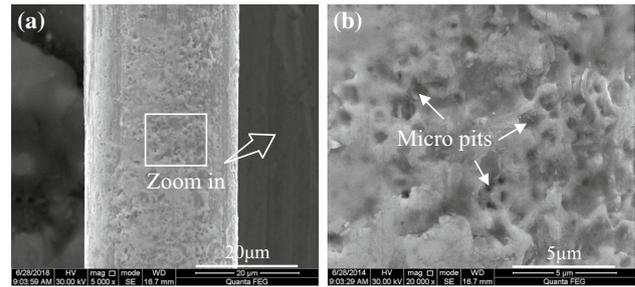
Fig. 14 SEM images of micro wire after machining: **a** overall view and **b** enlarged view

some are even in submicron. The diameters of the micro wire before and after machining are measured by microscope system VHX-6000 with 29.6 μm and 29.1 μm, respectively. The above reveal that the micro wire wear is negligible and it has little effect on machining accuracy.

5 Conclusions

In this study, the *MRR* and machining gap during machining SKD11 by micro reciprocated wire-EDM are investigated under different machining parameters including open voltage, discharge capacitance, pulse duration and feed rate. What's more, the optimal solutions are obtained based on NSGA-II, and finally a typical experimental sample is successfully machined with high machining accuracy. Detailed conclusions can be drawn below:

1. *MRR* initially increases with the increase of open voltage, and then tends to be constant when open voltage reaches a certain level. The reason is that high open voltage generates large discharge energy. But, overlarge one will lead to much material to be removed and debris particles accumulate in the machining gap, deteriorating the discharge state. The rise in discharge capacitance, pulse duration and feed rate cause high *MRR*. For machining gap, it increases with the increase of open voltage, discharge capacitance and pulse duration. That is because large discharge force and electromagnetic force are caused by high levels of the factors, resulting in fierce wire vibration. As for feed rate, the large one leads to the decrease of machining gap.

2. The mathematical models of *MRR* and machining gap are established by ANOVA, which are used to predict and optimize the output responses. Meanwhile, the verification experiments are conducted in the all 30 experiments and the deviation rate of *MRR* and machining gap are within 8.38% and 6.70%, respectively. Thus, it is concluded that the developed models are reliable. Subsequently, the multi-objective optimization based on

NSGA-II is carried out using the established functions and the pareto-optimal front is obtained.

3. To meet different machining performance, the optimal solutions are divided into three regions i.e. Region-A, B and C for small machining gap, compromised machining gap and *MRR*, and high *MRR*, respectively. One of the optimal machining conditions labelled No. 14 is used to machine the experimental sample i.e. micro gear. The unilateral machining gap with 3.83 µm is compensated in tool path and the micro gear with high machining accuracy of 1194.38 µm tip diameter is obtained.

References

1. Ghayesh, M., Farokhi, H., & Amabili, M. (2013). Nonlinear behaviour of electrically actuated MEMS resonators. *International Journal of Engineering Science, 71,* 137–155.
2. Zhong, J. M., Wu, X. Y., Xu, B., Li, J. B., Luo, F., Cheng, R., et al. (2015). Laminated fabrication of micro-stepped gear mold based on WEDM and thermal diffusion welding. *The International Journal of Advanced Manufacturing Technology, 78*(5–8), 1233–1240.
3. Li, J. W., Liu, H. X., Shen, Z. B., Qian, Q., Zhang, H. F., & Wang, X. (2016). Formability of micro-gears fabrication in laser dynamic flexible punching. *Journal of Materials Processing Technology, 234,* 131–142.
4. Zhang, Q., Felder, E., & Bruschi, S. (2009). Evaluation of friction condition in cold forging by using T-shape compression test. *Journal of Materials Processing Technology, 209*(17), 5720–5729.
5. Pandey, A., & Singh, S. (2010). Current research trends in variants of electrical discharge machining: A review. *International Journal of Engineering Science and Technology, 2*(6), 2172–2191.
6. Ho, K. H., Newman, S. T., Rahimifard, S., & Allen, R. D. (2004). State of the art in wire electrical discharge machining (WEDM). *International Journal of Machine Tools and Manufacture, 44*(12–13), 1247–1259.
7. Muthuramalingam, T., & Mohan, B. (2015). A review on influence of electrical process parameters in EDM process. *Archives of Civil and Mechanical Engineering, 15*(1), 87–94.
8. Park, J. W., Kim, B. H., Ok, J. G., Kim, W. J., Kim, Y. H., & Chu, C. N. (2012). Wire electrical discharge machining of carbon nanofiber mats for field emission. *International Journal of Precision Engineering and Manufacturing, 13*(4), 593–599.
9. Yilmaz, N. F., & Eyercioglu, O. (2008). An integrated computer-aided decision support system for die stresses and dimensional accuracy of precision forging dies. *The International Journal of Advanced Manufacturing Technology, 40*(9–10), 875–886.
10. Ming, W., Zhang, Z., Zhang, G., Huang, Y., Guo, J. W., & Chen, Y. (2014). Multi-objective optimization of 3D-surface topography of machining YG15 in WEDM. *Materials and Manufacturing Processes, 29*(5), 514–525.
11. Zhao, Y., Kunieda, M., & Abe, K. (2014). Study of EDM cutting of single crystal silicon carbide. *Precision Engineering, 38*(1), 92–99.
12. Ming, W., Zhang, Z., Wang, S. Y., Huang, H., Zhang, Y., & Shen, D. L. (2017). Investigating the energy distribution of workpiece and optimizing process parameters during the EDM of Al6061, Inconel718, and SKD11. *The International Journal of Advanced Manufacturing Technology, 92*(9–12), 4039–4056.
13. Zheng, J., Lai, X., Zhou, X., Chen, A., & Zheng, W. (2019). Non-pulsed energy modeling based on energy consumption subunits in wire electrical discharge machining (WEDM) process. *International Journal of Precision Engineering and Manufacturing, 20*(5), 853–862.
14. Sun, Y., Gong, Y., Liu, Y., Cai, M., Ma, X. T., & Li, P. F. (2018). Experimental investigation on effects of machining parameters on the performance of Ti–6Al–4 V micro rotary parts fabricated by LS-WEDT. *Archives of Civil and Mechanical Engineering, 18*(2), 385–400.
15. Di, S. C., Chu, X. Y., Wei, D. B., Wang, Z. L., Chi, G. X., & Liu, Y. (2009). Analysis of kerf width in micro-WEDM. *International Journal of Machine Tools and Manufacture, 49*(10), 788–792.
16. Habib, S., & Okada, A. (2015). Experimental investigation on wire vibration during fine wire electrical discharge machining process. *The International Journal of Advanced Manufacturing Technology, 4*(9–12), 2265–2276.
17. Habib, S., & Okada, A. (2016). Study on the movement of wire electrode during fine wire electrical discharge machining process. *Journal of Materials Processing Technology, 227,* 147–152.
18. Saha, A., & Mondal, S. C. (2016). Multi-objective optimization in WEDM process of nanostructured hardfacing materials through hybrid techniques. *Measurement, 94,* 46–59.
19. Khan, I. A., & Tikam, S. R. (2012). Modeling of wire electrical discharge machining of alloy steel (HCHCr). *International Journal of Precision Engineering and Manufacturing, 13*(11), 1989–1995.
20. Abidi, M. H., Al-Ahmari, A. M., Umer, U., & Rasheed, M. S. (2018). Multi-objective optimization of micro-electrical discharge machining of nickel-titanium-based shape memory alloy using MOGA-II. *Measurement, 125,* 336–349.
21. Zhenlong, W., Xuesong, G., Guanxin, C., & Yukui, W. (2014). Surface integrity associated with SiC/Al particulate composite by micro-wire electrical discharge machining. *Materials and Manufacturing Processes, 29*(5), 532–539.
22. Box, G. E. P., & Wilson, K. B. (1992). *On the experimental attainment of optimum conditions. Breakthroughs in statistics* (pp. 270–310). New York: Springer.
23. Deb, K., Pratap, A., Agarwal, S., & Meyarivan, T. (2002). A fast and elitist multiobjective genetic algorithm: NSGA-II. *IEEE Transactions on Evolutionary Computation, 6*(2), 182–197.
24. Guitrau, E. B. (1997). *The EDM handbook* (pp. 102–105). Cincinnati: Hanser Gardner.
25. Heo, S., Jeong, Y. H., Min, B. K., & Lee, S. J. (2009). Virtual EDM simulator: Three-dimensional geometric simulation of micro-EDM milling processes. *International Journal of Machine Tools and Manufacture, 49*(12–13), 1029–1034.
26. Jameson, E. C. (2001). *Electrical discharge machining* (pp. 82–85). Dearborn: Society of Manufacturing Engineers.

Publisher's Note Springer Nature remains neutral with regard to jurisdictional claims in published maps and institutional affiliations.

Xiang Chen PhD candidate at Harbin Institute of Technology, China. He is currently interested in the process research and development of micro-EDM and micro-WEDM.

Yukui Wang Associate professor at School of Mechatronics Engineering, Harbin Institute of Technology, China. His main research interests include micro-EDM control technique, robotics and Mitsubishi automation technology.

Zhenlong Wang Professor, a PhD candidate supervisor and deputy dean at School of Mechatronics Engineering, Harbin Institute of Technology, China. His main research interests include non-traditional machining, micro machining, and precision machining.

Guanxin Chi Professor at School of Mechatronics Engineering, Harbin Institute of Technology, China. His research interests mainly include micro EDM technology, multi-axis linkage CNC EDM system and EDM technology for special materials and special parts.